


 Cite this: *RSC Adv.*, 2021, 11, 927

# DFT studies of the CH<sub>4</sub>-SCR of NO on Fe-doped ZnAl<sub>2</sub>O<sub>4</sub>(100) surface under oxygen conditions

 Xiang Ren,  Honglin Tan,\* Qian Jie and Jianqi Liu

The catalytic reduction performance of NO on the surface of Fe-doped ZnAl<sub>2</sub>O<sub>4</sub> (100) was calculated based on DFT. The adsorption of NO and other molecules, the change of reaction energy of CH<sub>4</sub> and C<sub>2</sub>H<sub>4</sub> as reducing agents, and the activation energy barrier of CH<sub>4</sub> were studied. It was found that the best adsorption energy of NO is −2.166 eV. Compared with Al and Zn sites, doped Fe atoms are better adsorption catalytic sites. At temperatures of 300 K and 600 K, the molecules will move in the direction of the Fe atoms. O<sub>2</sub> adsorption will repel NO, reduce its adsorption energy, and cause NO to lose electrons and be oxidized. The reaction enthalpy with CH<sub>4</sub> as the reducing agent is −7.02 eV, and with C<sub>2</sub>H<sub>4</sub> is −3.45 eV. Transition state calculations show that O reduces the dissociation barrier of CH<sub>4</sub> by about 2 eV. The smaller adsorption energy and negative reaction enthalpy of the product indicate that the iron-doped ZnAl<sub>2</sub>O<sub>4</sub> has a good catalytic NO potential. This also provides a basis for future research on the catalytic mechanism of different hydrocarbons.

 Received 26th November 2020  
 Accepted 16th December 2020

DOI: 10.1039/d0ra10017j

[rsc.li/rsc-advances](https://rsc.li/rsc-advances)

## 1. Introduction

With economic development, pollution, especially air pollution, has been increasingly prevalent.<sup>1,2</sup> A large amount of NO<sub>x</sub> emissions come from coal-fired power and the use of automobiles. NO<sub>x</sub> is a harmful gas and is the main cause of air pollution, particularly in terms of acid rain. It also causes photochemical smog and does harm to people's health.<sup>3,4</sup> So it is important to study ways to cut NO<sub>x</sub> emissions. Selective catalytic reduction technology (SCR) is currently the most successful and widely used flue gas denitration technology. HC-SCR with hydrocarbon as a reducing agent has low catalytic reaction temperature and high catalytic activity in an oxygen-rich environment. The research and development of catalysts are among core issues surrounding SCR, and the performance of the catalyst directly affects the outcomes of NO<sub>x</sub> removal.<sup>5–9</sup>

Finding catalysts and reducing agents that have better performances and lower prices are focuses of the current research. The metal oxide catalyst is a kind of catalyst that is easy to obtain and has good catalytic properties. A complex oxide is composed of two or more metal oxides. It has better properties than a single oxide, with better stability, corrosion resistance, higher-temperature resistance, as well as more hardness compared with other properties. The development of composite oxides including spinel has become an important research area in the field of catalysis today. At present, spinel-type catalysts have a wide range of catalytic activation temperatures, good dispersibility, thermal stability, and hydrothermal

stability, and are particularly suitable for tail gas treatment of oxygen-rich lean burn.<sup>10–16</sup> He *et al.*<sup>17</sup> studied the selective catalytic reduction of NO<sub>x</sub> by BaAl<sub>2</sub>O<sub>4</sub> spinel under oxygen. The results show that at 673 K, the presence of oxygen reduces the light-off temperature of soot and promotes the conversion of NO<sub>x</sub>-N<sub>2</sub>. Xu *et al.*<sup>18</sup> stated that 0.05Pd-doped MAl<sub>2–x</sub>O<sub>4</sub> (M = Co, Cu, Zn) significantly improved the conversion of NO removal at 100–300 °C and 2% oxygen. It has been found that O<sub>2</sub>, which is ubiquitous in the air, has an inevitable effect on the catalytic removal of NO<sub>x</sub>.

In recent years, DFT calculation has been very extensive in predicting the structure and performance of catalysts.<sup>19,20</sup> For example, two-dimensional materials as single-site catalysts have been successfully designed for a variety of chemical reactions.<sup>21–24</sup> The adsorption performance is closely related to the catalysis.<sup>25–28</sup> At present, the adsorption performance of NO<sub>x</sub> on the spinel surface is calculated based on the first-principles method.<sup>29–33</sup> The effects of spinel-catalyzed species adsorption on the surface activity are investigated. Jiang *et al.*<sup>34</sup> used the first-principles VASP software to study the related properties of NO adsorbed on the surface of CuFe<sub>2</sub>O<sub>4</sub>(100) by N and O ends, respectively. Zou *et al.*<sup>27</sup> calculated the adsorption properties of NH<sub>3</sub> on the ZnFe<sub>2</sub>O<sub>4</sub> surface. Xiang<sup>35,36</sup> found that the property of NO<sub>2</sub> and NO adsorbed on ZnGaAlO<sub>4</sub>(100) surface.

An important member of the AB<sub>2</sub>O<sub>4</sub> spinel oxide family is ZnAl<sub>2</sub>O<sub>4</sub>, which is called zinc aluminate. This material is a wide band-gap material with an energy gap of about 4 eV at room temperature. ZnAl<sub>2</sub>O<sub>4</sub> has many interesting properties, making it an ideal choice for use in different potential fields. At present, there are few studies on the catalytic reduction of NO by aluminum–zinc spinel. The doping of transition metal elements

Faculty of Materials Science and Engineering, Kunming University of Science and Technology, Kunming 650093, China. E-mail: 852419171@qq.com



has a significant improvement in the catalytic effect. In this paper, Fe-doped ZnAl<sub>2</sub>O<sub>4</sub> is used as a catalyst to study the adsorption performance of NO and other gas molecules on the (100) surface by density functional theory. Then the energy change of the surface reaction and the dehydrogenation barrier of CH<sub>4</sub> were calculated. This study attempted to delve into its catalytic mechanism, studying whether it can be used as a good catalyst, and the role of oxygen in the reaction.

## 2. Computational details and crystal structure

The First-principles calculations were conducted using Materials-Studio with exchange-correlation potential effects treated by the generalized gradient approximation (GGA) by Perdew–Burke Ernzerhof (PBE). The Dmol3 module of Material Studio based on density functional theory is used to calculate the adsorption structure and electronic structure. To facilitate the geometry optimization progress, the convergence criteria for the energy, force, and displacement were set at  $1.0 \times 10^{-5}$  Ha,  $0.001 \text{ Ha } \text{Å}^{-1}$ , and  $0.001 \text{ Å}$ , respectively. The Brillouin zone was set at  $3 \times 3 \times 1$ . The calculation uses a spin non-limiting method, with a valence electron wave function and a polarization function plus a double-valued basis set expansion (DNP). For Zn, Al, Fe, O, N atoms, effective core potential treatment (ECP) was adopted and Al-3s3p, Zn-3p3d4s, Fe-3d4s were treated as valence electrons states. A super-soft description was used between core and valence electrons. To balance the computational cost and accuracy of the calculations, a Hexadecapole polarization potential deployment was used with a Fermi tailing effect of 0.008 Hartree and an orbital intercept radius of  $4.8 \text{ Å}$ . To test the stability of NO molecules on the surface at ambient temperature, *ab initio* MD as implemented in Dmol<sup>3</sup> simulations have been carried out. NVT (N, V, and T are the constant number of atoms, constant volume, and constant temperature, respectively) ensemble is selected and the Nose–Hoover thermostat method is used to control the temperature at 300 K without external pressure in the calculation. The simulation time step is set at 1 fs and the total simulation time is 1.5 ps to enable the calculation finish within a reasonable time range. The transition states were located using the complete linear synchronous transit/quadratic synchronous transit (LST/QST) method. And the frequencies of them are examined to confirm the validity.

We first calculated the lattice structure of ZnAl<sub>2</sub>O<sub>4</sub>,  $a = 8.2188$ ,  $b = 8.1843$ ,  $c = 8.2335$ ;  $\alpha = \beta = \gamma = 90.0^\circ$ , which is in good agreement with other data. We know that there are tetrahedral and octahedral positions in the crystal lattice, and Fe can replace Zn and Al atoms respectively. Nimai Pathak found that iron tends to occupy tetrahedral sites when doped at low concentrations. M. A. Lahmer also found through calculations that replacing aluminum with iron atoms is more stable than replacing zinc.<sup>37,38</sup> Considering that it is easier to dope on the surface, we choose to dope Fe to Al sites near the surface, as shown in Fig. 1(a).<sup>39</sup> The lattice constant of Fe-doped ZnAl<sub>2</sub>O<sub>4</sub> (the following are expressed with Fe/ZnAl<sub>2</sub>O<sub>4</sub>) is slightly increased, and the lattice is still a face-centered cubic structure. For all the figures in this article: red for O, blue for N, green for

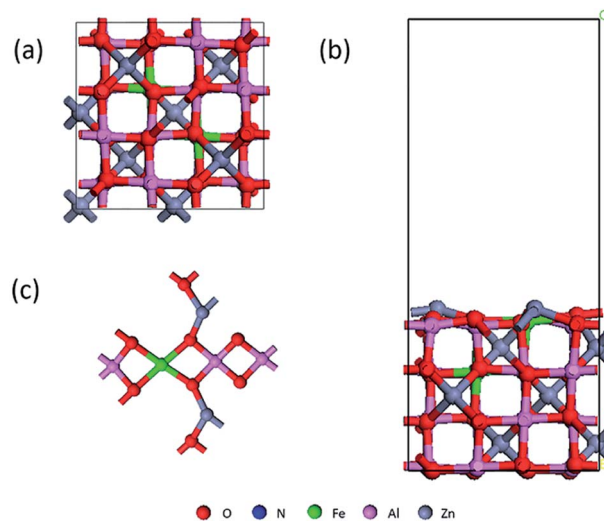


Fig. 1 (a) Crystal structure of Fe/ZnAl<sub>2</sub>O<sub>4</sub> (b) side view of Fe/ZnAl<sub>2</sub>O<sub>4</sub> (100) surface model (c) surface layer top view. For all the figures in this article: red for O, blue for N, green for Fe, pink for Al, and gray for Zn.

Fe, pink for Al, and gray for Zn. We cut the surface of the low-index surface (100) and chose to expose the indicator layer with more metal atoms because it is more beneficial to the catalytic reaction.

The vacuum region thickness of  $15 \text{ Å}$  was chosen to eliminate the interaction effects of the neighboring slab. The optimized structure is shown in Fig. 1(b), and then we perform the adsorption calculation. The expression of the adsorption energy is:

$$E_{\text{ads}} = E_{\text{molecule+slab}} - E_{\text{slab}} - E_{\text{molecule}}$$

Among them,  $E_{\text{molecule+slab}}$ ,  $E_{\text{slab}}$ , and  $E_{\text{molecule}}$  are the total energy of the adsorbed molecules and surface models, the energy of the surface model, and the energy of a single adsorbed molecule respectively.

## 3. Results and discussion

Two kinds of stable adsorption structures were obtained by optimizing the adsorption of NO on the surface of Fe/ZnAl<sub>2</sub>O<sub>4</sub>: (1) the adsorption configuration of N-down adsorption, as shown in Fig. 2(a–c); (2) the adsorption configuration of O-down adsorption, as shown in Fig. 2(d–f). It can be seen from Fig. 2 the N or O atoms have different adsorption bond lengths on the metal atoms. Among them, the N–Fe adsorption bond has the shortest length, and the N-end adsorption on the Fe site has the strongest adsorption strength in single-ended adsorption. This is consistent with Xiang Chao's research on ZnGaAlO<sub>4</sub>(100) and Pâmella's research on Co<sub>3</sub>O<sub>4</sub>(100) surface.<sup>35</sup>

It can be seen from Fig. 3 that the adsorption energy of the O terminal of NO is  $-1.230 \text{ eV}$  to  $-1.397 \text{ eV}$ , while the adsorption energy at the N terminal is higher, the value is  $-1.578 \text{ eV}$  to  $-2.118 \text{ eV}$ . The positive adsorption energy is expressed as an endothermic process, and the adsorption structure is



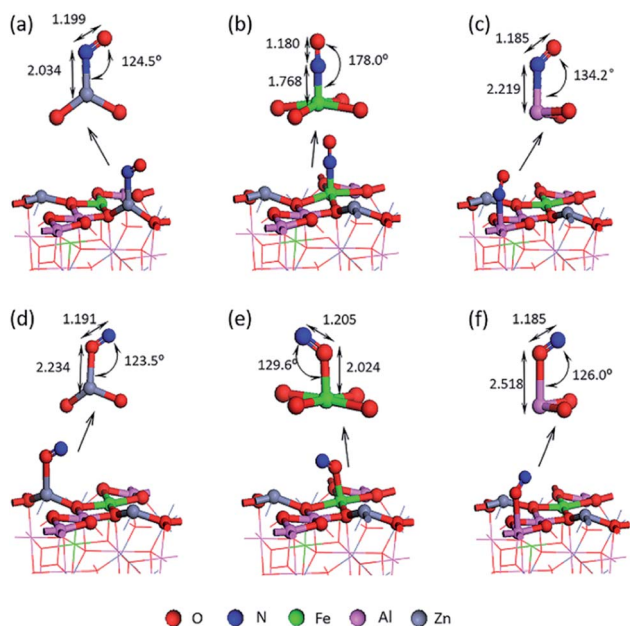


Fig. 2 Single-ended adsorption structure of NO adsorbed on the surface (a) Zn-NO; (b) Fe-NO; (c) Al-NO; (d) Zn-ON; (e) Fe-ON and (f) Al-ON.

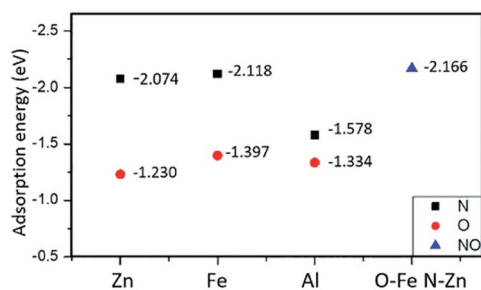


Fig. 3 Adsorption energy at different adsorption sites.

thermodynamically unstable. All the adsorption energy is negative, indicating that the process is exothermic, and the corresponding adsorption structure is stable.

The bonding mechanism diagram of NO molecule is shown in Fig. 4. (a) is the PDOS of the N and O atoms before the adsorption of NO molecules, and the 3d orbital of the surface Fe, (b) the PDOS diagram of the O-end adsorption on Fe, and (c) the PDOS diagram of the N-end adsorption on Fe. It can be seen that the Fe 3d on the surface of Fe/ZnAl<sub>2</sub>O<sub>4</sub> (100) has an energy level on both sides of the Fermi surface. After adsorption, the 3d peak of Fe is severely cleaved, and the p-orbital of NO and the 3d orbital of Fe atom are strongly hybridized near the Fermi surface, and the energy levels are all shifted to the left, demonstrating that the adsorption produces a strong interaction. Moreover, the intensity of the Fe-3d peak becomes small, which means that electrons are transferred from the surface Fe to the NO molecule. According to the change of static charge value, the charge changes of the seven kinds of NO adsorbed on the surface structure in Fig. 2 are  $-0.132 e$ ,  $-0.112 e$ ,  $-0.155 e$ ,  $-0.161 e$ ,  $-0.230 e$ ,  $-0.145 e$ ,  $-0.247 e$ . It also proves that charge is transferred from the surface to the gas molecules.

We calculated the adsorption energy of different double-end adsorption on the surface and found that it is most stable when adsorbed by the N-Zn O-Al structure (as shown in Fig. 5(a)). It has the largest adsorption energy of  $-2.166 eV$ . At this time, the N-O bond length is  $1.226 \text{ \AA}$ . Compared with the free state NO, the N-O bond length is  $0.062 \text{ \AA}$  (the maximum elongation), and the surface NO has a strong interaction with the surface. Fig. 5 shows the calculated molecular dynamics at 300 K and 600 K. It was found that as the temperature increased, the molecules tilted towards Fe atoms. Generally, high temperature will increase the atomic distance and weaken the strength, but the Fe-O bond length even decreases at 300 K, which may prove that Fe atoms have a better high-temperature adsorption performance.

Fig. 6(a) shows the most stable adsorption state of a single O<sub>2</sub> on the Fe/ZnAl<sub>2</sub>O<sub>4</sub> (100) surface. We intend to study the catalytic effect under oxygen-rich conditions, so we would consider the

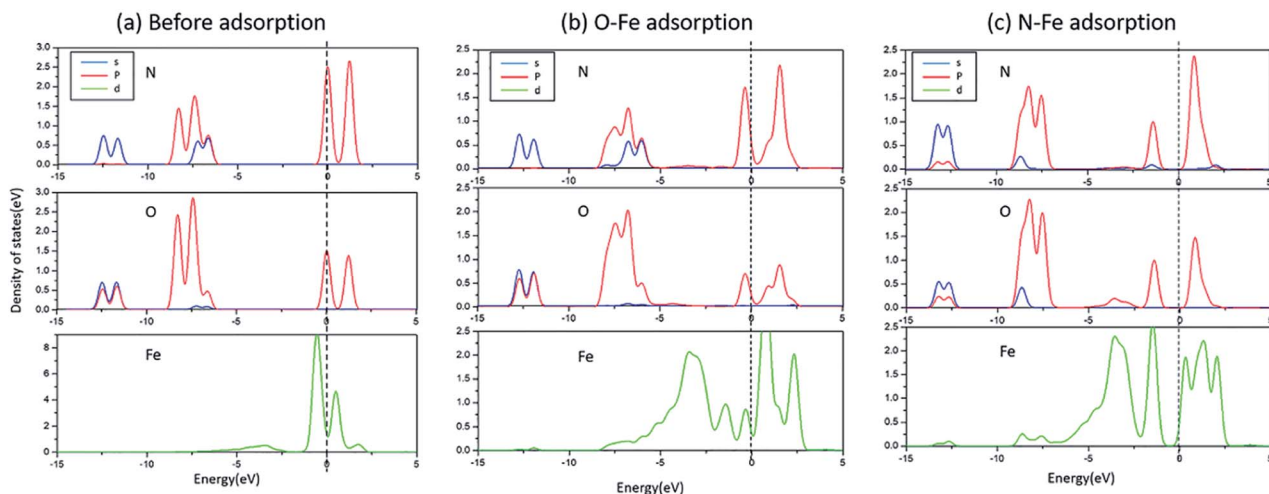


Fig. 4 The PDOS of N, O, and Fe in different situations (a) before adsorption; (b) O-Fe adsorption; (c) N-Fe adsorption.



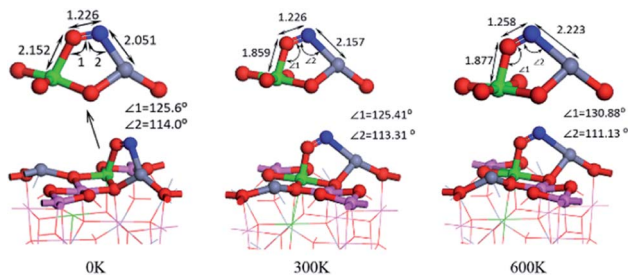


Fig. 5 NO double coordination adsorption configuration at 0 K, 300 K, 600 K.

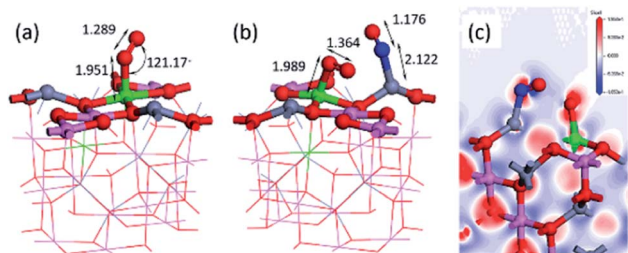


Fig. 6 (a) Most stable  $O_2$  adsorption structure, (b) NO,  $O_2$  co-adsorption structure and (c) the differential charge density map.

Table 1 The  $E_{\text{ads}}$ ,  $E_{\text{inter}}$ , and charges of co-adsorption

	$E_{\text{ads}}$ (eV)	$E_{\text{inter}}$ (eV)	Charges change ( $ e $ )
NO	-2.16	—	-0.12
$O_2$	-4.21	—	-0.37
NO $O_2$	-2.85	1.184	NO 0.022/ $O_2$ -0.584

effect of adsorption on NO in the presence of oxygen. First, we calculated the adsorption energy of oxygen in different sites and found the best adsorption site. When  $O_2$  is adsorbed on Fe, the adsorption bond length is the shortest and the adsorption capacity is the strongest. The adsorption energy can reach -4.21 eV, and the distance between O and surface Fe is 1.952 Å, which is the shortest among all adsorption sites. The distance between the two oxygen atoms is 1.289 Å, which is 0.063 Å longer than the 1.226 Å before adsorption. This is due to the increase in bond length caused by the attraction of the surface to the molecules. We performed a co-adsorption calculation

and the results are shown above. Fig. 6(b) shows the structure after the co-adsorption of NO and  $O_2$ . The NO-N end is adsorbed at the Zn position, which is consistent with the original. The N-Zn distance is 2.122 Å, and the distance between NO is 1.176 Å. Compared with the single adsorption NO, the intramolecular distance becomes shorter, and the distance from the surface Zn becomes longer. The reason may be that the co-adsorption of  $O_2$  causes a certain repulsion between the molecules. The NO single adsorption is preferably N-Zn O-Fe, and at this time, due to the presence of  $O_2$ , the O atom of NO is not bent to this side, which proves that there is a repulsive effect. The total adsorption energy of the two molecules is -2.85 eV, which is lower than the adsorption energy of the two single adsorptions. The interaction between NO and  $O_2$  can be calculated by expression:

$$E_{\text{inter}} = E_{\text{slab+NO+O}_2} - E_{\text{slab+NO}} - E_{\text{slab+O}_2} + E_{\text{slab}}$$

where  $E_{\text{slab+NO+O}_2}$  is the total energy of the system composed of adsorbed molecules (NO and  $O_2$ ) and surface model;  $E_{\text{slab+NO}}$  is the total energy of adsorbed molecular NO and surface model;  $E_{\text{slab+O}_2}$  is composed of adsorbed molecule  $O_2$  and surface model total energy;  $E_{\text{slab}}$  is the total energy of the configuration. The calculated interaction energy is +1.184 eV, and its value is positive, indicating that NO and  $O_2$  have repulsion on the surface.

The charge distribution can be seen from Table 1 and Fig. 6(c) differential charge diagram. When NO is adsorbed on the surface, the surface metal atoms lose electrons, and NO gets electrons. However, when co-adsorbed with  $O_2$ ,  $O_2$  has a strong electron-withdrawing ability, and the electrons that lead to NO adsorption are plundered by  $O_2$ . The charge amount of NO is changed from -0.16 e to 0.022 e, and the charge of  $O_2$  is changed from -0.307 e to -0.584 e, which proves that the presence of  $O_2$  causes NO to be deactivated and oxidized. Many people have researched and found this phenomenon, such as Ingrid Castellanos found that the  $NO_2$  peak will appear when NO is adsorbed on Fe-HFER.<sup>40</sup> Zekang Lyu *et al.*'s research on  $\alpha$ - $Fe_2O_3$  (0 0 1) also found that the surface acidity increases after the transition metal is doped, and NO is more easily oxidized.<sup>41</sup>

To predict the reaction of NO on its surface, we also calculated the adsorption of other gas molecules related to the reaction, such as  $CH_4$ ,  $C_2H_4$ , and the product  $N_2$  and  $H_2O$ . The structure and key length data can be seen in Fig. 7 and Table 2. We can find that  $N_2$  and  $H_2O$  as the product have low adsorption capacity on the surface, which is beneficial to the desorption process of the product and prevents its catalytic poisoning. The structural diagrams of  $CH_4$  and  $C_2H_4$  show that they are far

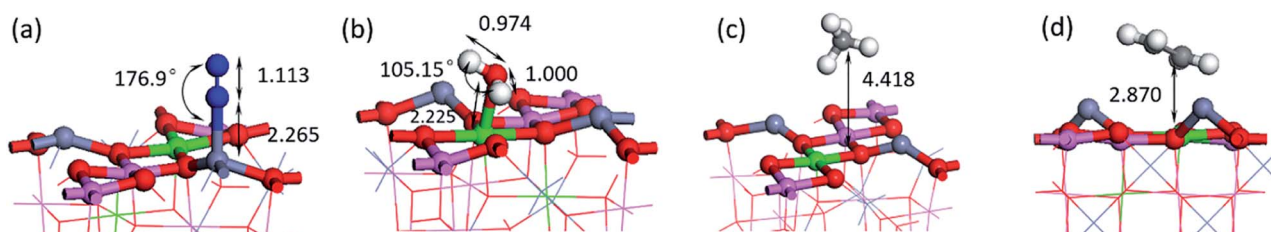
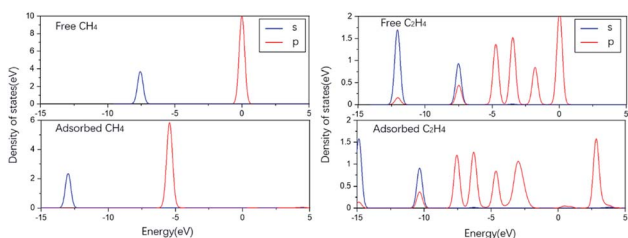


Fig. 7 The most stable adsorption structure of other molecules (a)  $N_2$  (b)  $H_2O$  (c)  $CH_4$  (d)  $C_2H_4$ .



Table 2 The  $E_{\text{ads}}$  and  $d_{\text{m-s}}$  of different adsorption structure

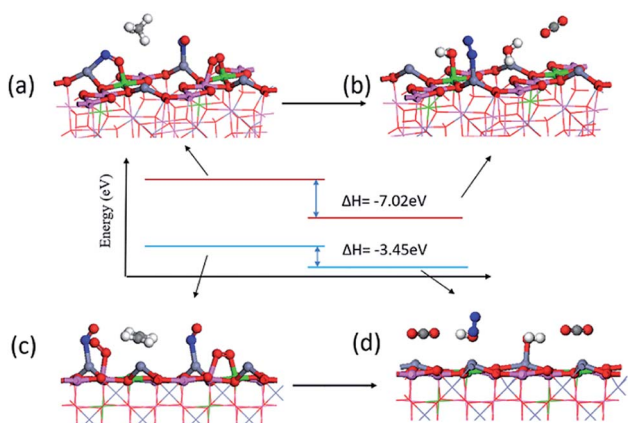
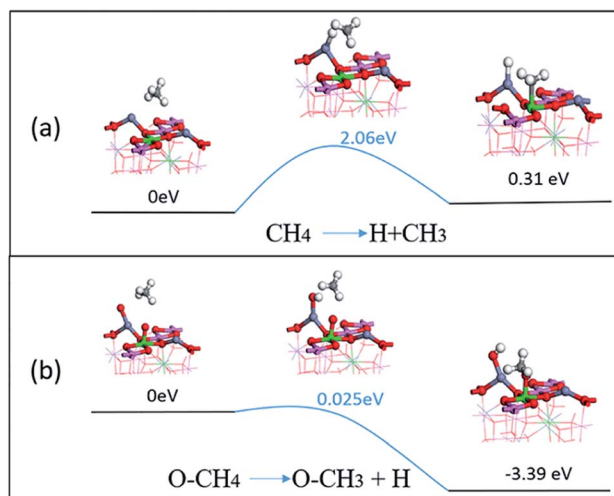
	$E_{\text{ads}}$ (eV)	$d_{\text{m-s}}$ (Å)
$\text{N}_2$	-0.58	2.265
$\text{H}_2\text{O}$	-1.18	2.225
$\text{CH}_4$	-0.57	4.418
$\text{C}_2\text{H}_4$	-3.42	2.870

Fig. 8 The PDOS of  $\text{CH}_4$ ,  $\text{C}_2\text{H}_4$  free and adsorbed respectively.

away from the surface and are not shown to be bonded. It can be seen from the PDOS diagram in Fig. 8 that the orbital shape of the C atom before and after adsorption does not change, but all shift to the low energy direction. This phenomenon can also be seen on the adsorption of many molecules.

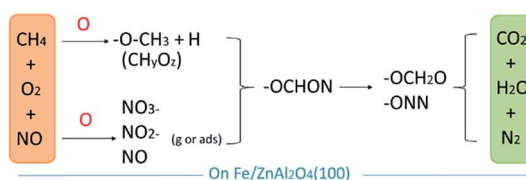
The adsorption performance of the reducing agent  $\text{NH}_3$  on various surfaces has been extensively calculated by many researchers. Its strong adsorption and charge transfer are effective prerequisites for molecular activation and promotion of reactions. However, many experimental studies have proved that  $\text{CH}_4$  is one of the good reducing agents, even if it has poor adsorption. We can use the following method to do a brief verification.

As shown in Fig. 9, since it is difficult to adsorb many molecules on the surface of a single unit cell at the same time, we established a  $2 \times 1$  unit cell surface model to adsorb the reactant product molecules according to their stable adsorption sites. The total energy change before and after the surface

Fig. 9 Structure and enthalpy change of energy of product and reactant (a) the reactants of NO reduction by  $\text{CH}_4$ , (b) product of NO reduction by  $\text{CH}_4$ , (c) the reactants of NO reduction by  $\text{C}_2\text{H}_4$ , (d) product of NO reduction by  $\text{C}_2\text{H}_4$ .Fig. 10 The dissociation energy of  $\text{CH}_4$  changes on (a) a clean surface; (b) a surface with O atoms.

reaction can be obtained to understand the difficulty of the reaction to a certain extent. The reaction from (a) to (b) is  $\text{CH}_4 + 2\text{NO} + \text{O}_2 = \text{N}_2 + 2\text{H}_2\text{O} + \text{CO}_2$ . The calculated reaction enthalpy becomes  $-7.02$  eV, which is a relatively high value. Prove that the reaction is easy to proceed. The reaction from (c) to (d) is  $\text{C}_2\text{H}_4 + 2\text{NO} + 2\text{O}_2 = \text{N}_2 + 2\text{H}_2\text{O} + 2\text{CO}_2$ , and the reaction enthalpy change is only  $-3.45$  eV. Gibbs free energy is the best parameter to measure whether the reaction can proceed, but the substances before and after the reaction are all four molecules adsorbed on the surface. The adsorption process is caused by electron transfer and attraction on the surface. The desorption of the final product is caused by the increase in entropy at a certain temperature. The enthalpy change shows the energy change of the reaction after the molecules are adsorbed on the surface.

From the adsorption and dissociation barriers of  $\text{CH}_4$  on the surface, it can be seen that methane is a stable molecule, which is difficult to activate in the reaction. As shown in Fig. 10(a),  $\text{CH}_4$  removes an H atom from the surface, and the energy barrier of 2.06 eV needs to be overcome, and the  $-\text{CH}_3$  energy of the subsequent structure is also greater than the original molecule. This proved that its molecules will not activate and decompose on the surface. But the presence of oxygen can greatly reduce the decomposition barrier. As shown in Fig. 10(b), surface oxygen atoms can come from the decomposition of oxygen or diffuse to the surface from the spinel lattice. The  $\text{CH}_4$  dissociates an H in this case and only needs a 0.025 eV barrier and the energy of the subsequent

Fig. 11 Schematic diagram of the reaction process of possible  $\text{CH}_4$ -SCR of NO.

adsorption state is also more stable, at  $-3.39$  eV. The presence of oxygen atoms on the surface will greatly promote the activation and dissociation of  $\text{CH}_4$ , which in turn will cause subsequent reduction reactions with NO or nitrate.

Finally, the general process of NO catalyzing on the  $\text{Fe}/\text{ZnAl}_2\text{O}_4$  surface is shown in Fig. 11. Oxygen can promote the formation of nitrates from NO, and it can also promote the activation and decomposition of  $\text{CH}_4$ . Then the two have subsequent reactions, gradually reducing to produce  $\text{N}_2$ ,  $\text{H}_2\text{O}$ , and  $\text{CO}_2$ .

## 4. Conclusions

The adsorption configuration of NO, and other molecules on the surface of  $\text{Fe}/\text{ZnAl}_2\text{O}_4$  (100) was constructed based on DFT. The optimized structures and energy of each adsorption site were calculated. It is found that for NO, the adsorption effect at the N-terminus is stronger than that at the O-terminus, and the optimal adsorption site is the doped Fe atom. The adsorption effect of Fe end is still strong at 300 K and 600 K. It also describes the repulsion phenomenon that occurs when NO and  $\text{O}_2$  coexist.  $\text{O}_2$  attracts NO electrons, reducing its adsorption effect and producing an oxidation effect. Using  $\text{CH}_4$  and  $\text{C}_2\text{H}_4$  as reducing agents, this study calculated the reduction enthalpy of NO in  $\text{Fe}/\text{ZnAl}_2\text{O}_4$  (100). It is found that they are both exothermic reactions and prone to reactions. The stable  $\text{CH}_4$  molecules have better catalytic properties instead. We have studied its dissociation ability and found that the presence of O can lower the energy barrier of 2 eV and greatly promote the activation of  $\text{CH}_4$ . The results show that  $\text{Fe}/\text{ZnAl}_2\text{O}_4$  has a good potential for  $\text{CH}_4$ -SCR to catalyze NO on oxygen conditions.

## Author contributions

Honglin Tan: conceptualization, methodology, funding acquisition, writing – review & editing, Xiang Ren: data curation, writing – original draft, formal analysis, Jie Qian: data curation, formal analysis, Investigation, Jianqi Liu: visualization, investigation, validation.

## Conflicts of interest

The authors declare that they have no conflict of interest.

## Acknowledgements

This work was supported by the National Natural Science Foundation of China (51662023).

## References

- 1 S. Roy, M. S. Hegde and G. Madras, *Appl. Energy*, 2009, **86**, 2283–2297.
- 2 Y.-q. Wang, X.-f. Yan, W. Xiao and Y.-x. Shao, *Bull. Korean Chem. Soc.*, 2017, **38**, 625–631.
- 3 T. Boningari and P. G. Smirniotis, *Curr. Opin. Chem. Eng.*, 2016, **13**, 133–141.

- 4 P. Granger and V. I. Parvulescu, *Chem. Rev.*, 2011, **111**, 3155–3207.
- 5 M. Kantcheva and A. S. Vakkasoglu, *J. Catal.*, 2004, **223**, 352–363.
- 6 M. Fu, C. Li, P. Lu, L. Qu, M. Zhang, Y. Zhou, M. Yu and Y. Fang, *Catal. Sci. Technol.*, 2014, **4**, 14–25.
- 7 F. Gao, X. Tang, H. Yi, S. Zhao, C. Li, J. Li, Y. Shi and X. Meng, *Catalysts*, 2017, **7**, 199.
- 8 C. Niu, J. Niu, S. Wang, Z. Wang, S. Dong, H. Fan, Y. Hong and D. Liu, *Catal. Commun.*, 2019, **123**, 49–53.
- 9 G. Xu, J. Ma, L. Wang, W. Xie, J. Liu, Y. Yu and H. He, *Appl. Catal., B*, 2019, **244**, 909–918.
- 10 S. Yang, J. Li, C. Wang, J. Chen, L. Ma, H. Chang, L. Chen, Y. Peng and N. Yan, *Appl. Catal., B*, 2012, **117–118**, 73–80.
- 11 M. Zawadzki, W. Walerczyk, F. E. López-Suárez, M. J. Illán-Gómez and A. Bueno-López, *Catal. Commun.*, 2011, **12**, 1238–1241.
- 12 S. G. Menon, K. S. Choudhari, S. A. Shivashankar, C. Santhosh and S. D. Kulkarni, *J. Alloys Compd.*, 2017, **728**, 1083–1090.
- 13 D. Fino, N. Russo, G. Saracco and V. Specchia, *J. Catal.*, 2006, **242**, 38–47.
- 14 M. Yuan, Y. Su, W. Deng and H. Zhou, *Chem. Eng. J.*, 2019, **375**, 122091.
- 15 D. Yadav, P. Singh and R. Prasad, *Int. J. Hydrogen Energy*, 2018, **43**, 5346–5357.
- 16 M. A. Lahmer, *Surf. Sci.*, 2018, **669**, 189–197.
- 17 H. Lin, Y. Li, W. Shangguan and Z. Huang, *Combust. Flame*, 2009, **156**, 2063–2070.
- 18 C. Xu, W. Sun, L. Cao, T. Li, X. Cai and J. Yang, *Chem. Eng. J.*, 2017, **308**, 980–987.
- 19 L.-M. Y. Jin-Hang Liu and E. Ganz, *ACS Sustainable Chem. Eng.*, 2018, **6**, 15494–15502.
- 20 J. Yang, X. L. Wang, Y. Qu, X. Wang, H. Huo, Q. Fan, J. Wang, L.-M. Yang and Y. Wu, *Adv. Energy Mater.*, 2020, **10**, 2001709.
- 21 L.-M. Yang, V. Bačić, I. A. Popov, A. I. Boldyrev, T. Heine, T. Frauenheim and a. E. Ganz, *J. Am. Chem. Soc.*, 2015, **137**, 2757–2762.
- 22 Y. Z. Bingyi Song, H.-M. Yang, Ji-H. Liao, Li-M. Yang, X.-B. Yang and E. Ganz, *J. Am. Chem. Soc.*, 2019, **141**, 3630–3640.
- 23 J.-H. Liu, L.-M. Yang and E. Ganz, *J. Mater. Chem. A*, 2019, **7**, 3805–3814.
- 24 J.-H. Liu, L.-M. Yang and E. Ganz, *J. Mater. Chem. A*, 2019, **7**, 11944–11952.
- 25 D. Fang, D. Li, F. He, J. Xie, C. Xiong and Y. Chen, *Comput. Mater. Sci.*, 2019, **160**, 374–381.
- 26 D. Ren and K. Gui, *Appl. Surf. Sci.*, 2019, **487**, 171–179.
- 27 C.-y. Zou, W. Ji, Z. Shen, Q. Tang and M. Fan, *Appl. Surf. Sci.*, 2018, **442**, 778–786.
- 28 X. C. Li and H. W. Gao, *Materials*, 2019, **12**, 1379.
- 29 B. Zhu, Q. Fang, Y. Sun, S. Yin, G. Li, Z. Zi, T. Ge, Z. Zhu, M. Zhang and J. Li, *J. Mater. Sci.*, 2018, **53**, 11500–11511.
- 30 Z. Artuc, H. Ustunel and D. Toffoli, *RSC Adv.*, 2014, **4**, 48492–48506.
- 31 H. Gao and Z. Liu, *RSC Adv.*, 2017, **7**, 13082–13091.



## Paper

- 32 L. P. Cui, J. T. Liu, S. Z. Liu, M. F. Wang, Z. H. Gao, Z. J. Zuo and W. Huang, *J. Mol. Model.*, 2018, **24**, 65.
- 33 Z. M. Liu, L. L. Ma and A. S. M. Junaid, *J. Phys. Chem. C*, 2010, **114**, 4445–4450.
- 34 Z. Jiang, W. Zhang, W. Shangguan, X. Wu and Y. Teraoka, *J. Phys. Chem. C*, 2011, **115**, 13035–13040.
- 35 C. Xiang, H. Tan, J. Lu, L. Yu, P. Song, C. Zeng, D. Zhang and S. Tao, *Phys. Scr.*, 2014, **89**, 075401.
- 36 C. Xiang, H. Tan, J. Lu, L. Yu, P. Song, C. Zeng, Y. Liang, S. Tao and Z. Chen, *Appl. Surf. Sci.*, 2015, **349**, 138–146.
- 37 M. A. Lahmer, *Comput. Condens. Matter*, 2019, **20**, e00387.
- 38 N. Pathak, S. K. Gupta, K. Sanyal, M. Kumar, R. M. Kadama and V. Natarajana, *Dalton Trans.*, 2014, **43**, 9313–9323.
- 39 A. B. F. Zerarga, R. Khenata and S. Bin-Omran, *Solid State Sci.*, 2011, **13**, 1638–1648.
- 40 O. M. Ingrit Castellanos, *Appl. Catal., B*, 2018, **223**, 143–153.
- 41 S. N. Zekang Lyua, C. Lua, G. Zhaob, Z. Gongga and Y. Zhuc, *Fuel*, 2020, **267**, 117147.

